Draft version April 2, 2015
Preprint typeset using LaTeX style emulateapj v. 01/23/15

M-M PAPER, MORPHOLOGICAL BIAS

G. A. D. Savorgnan[1] and A. W. Graham[1] and A. Marconi and E. Sani and L.K. Hunt
Centre for Astrophysics and Supercomputing, Swinburne University of Technology, Hawthorn, Victoria 3122, Australia.
Draft version April 2, 2015

ABSTRACT

We have the best latest M-L and M-M diagrams (66 galaxies = biggest sample ever used, IR imaging = minimally affected by dust and star formation, state-of-the-art multicomponent galaxy decompositions = we fit bulges, disks, spiral arms, bars, rings, haloes, extended or unresolved nuclear sources and partially depleted cores). Previous samples were overwhelmingly dominated by early-type galaxies, our sample includes 17 spiral galaxies, half of which have $M_{\rm BH} < 10^7 M_\odot$, thus we can explore the low-mass end of the diagrams. We provide a table with spheroid luminosities, spheroid stellar masses and galaxy luminosities. We give updated linear regressions for Sersic/core-Sersic galaxies and for different morphological types (E/S0, Sp). Sersic and core-Sersic galaxies have slopes consistent with each other (contrary to what claimed by GS13). In the M-M diagram, bulges of early type galaxies have a slope of ∼1, while bulges of spiral galaxies have a slope of 2-3. Linear regressions that we provide are symmetrical (to be compared with theoretical expectations) and non-symmetrical (to be used to predict BH masses). Contrary to a previous claim, the bulge luminosity appears to be a better indicator of the BH mass than the galaxy luminosity. Bulges with $n < 2$, claimed by some to be pseudobulges, are not offset to lower BH masses from the correlation defined by bulges with $n > 2$.
Subject headings: keywords

1. INTRODUCTION

More than two and a half decades ago, Dressler (1989) foresaw a "rough scaling of black hole mass with the mass of the spheroidal component", as suggested by the sequence of five galaxies (M87, M104, M31, M32 and the Milky Way). His "rough scaling" was a premature version of the nowadays popular correlation between black hole mass, $M_{\rm BH}$, and host spheroid luminosity, $L_{\rm sph}$, and also host spheroid mass, $M_{\rm sph}$ (Yee 1992; Kormendy & Richstone 1995; Magorrian et al. 1998; Marconi & Hunt 2003; Häring & Rix 2004). These early studies were dominated by high-mass, early-type galaxies, for which they reported a quasi-linear $M_{\rm BH} - M_{\rm sph}$ relation, consistent with a dry-merging formation scenario. Subsequent studies of the $M_{\rm BH} - L_{\rm sph}$ and $M_{\rm BH} - M_{\rm sph}$ diagrams (Ferrarese & Ford 2005; Lauer et al. 2007a; Graham 2007, 2008; Gültekin et al. 2009; Sani et al. 2011; Beifiori et al. 2012; Erwin & Gadotti 2012; Vika et al. 2012; van den Bosch et al. 2012; McConnell & Ma 2013; Kormendy & Ho 2013; Rusli et al. 2013a; see Graham 2015 for an extensive review about the early discovery and successive improvements of these correlations) used similar galaxy samples, which remained dominated by high-mass, early-type objects having $M_{\rm BH} \gtrsim 0.5 \times 10^8$ M$_\odot$, and recovered a near-linear relation. However, the consensus about a linear $M_{\rm BH} - M_{\rm sph}$ correlation was not unanimous. Some studies reported a slope steeper than one, or noticed that low-mass spheroids were downwards offset from the relation traced by their high-mass counterparts (Laor 1998; Wandel 1999; Laor 2001; Ryan et al. 2007). Recently, Läsker et al. (2014a,b) derived 2.2 μm bulge luminosities for 35 galaxies (among which only 4 were classified as spiral galaxies), and reported a slope below unity for their $M_{\rm BH} - M_{\rm sph}$ relation. They also claimed that the black hole mass correlates equally well with the total galaxy luminosity as it does with the bulge luminosity.

The $M_{\rm BH} - L_{\rm sph}$ relation can be predicted from other two correlations involving the bulge velocity dispersion, σ. The first of these two is the $M_{\rm BH} - \sigma$ relation (Ferrarese & Merritt 2000; Gebhardt et al. 2000), which can be described by a single power-law ($M_{\rm BH} \propto \sigma^5$) over the range in velocity dispersion $70 - 350$ km s^{-1} (e.g. Graham et al. 2011; McConnell et al. 2011; Graham & Scott 2013). The second is the $L_{\rm sph} - \sigma$ relation, which has long been known to be a "double power-law", being $L_{\rm sph} \propto \sigma^5$ at the luminous end (Schechter 1980; Malumuth & Kirshner 1981; von der Linden et al. 2007; Liu et al. 2008), and $L_{\rm sph} \propto \sigma^2$ at intermediate and faint luminosities (Davies et al. 1983; Held et al. 1992; Matković & Guzmán 2005; de Rijcke et al. 2005; Balcells et al. 2007; Chilingarian et al. 2008; Forbes et al. 2008; Cody et al. 2009; Tortora et al. 2009; Kourkchi et al. 2012). The change in slope of the $L_{\rm sph} - \sigma$ relation occurs at $M_B \approx -20.5$ mag, corresponding to $\sigma \approx 200$ km s^{-1}. That is, the $M_{\rm BH} - L_{\rm sph}$ relation should be better described by a "broken", rather than a single, power-law, having $M_{\rm BH} \propto L_{\rm sph}^{2.5}$ at the low-luminosity end, and $M_{\rm BH} \propto L_{\rm sph}^{1}$ at the high-luminosity end. Due to the scatter in the $M_{\rm BH} - L_{\rm sph}$ (or $M_{\rm BH} - M_{\rm sph}$) diagram, studies that have not sufficiently probed below $M_{\rm BH} \approx 10^7$ M$_\odot$ can easily miss the change in slope occuring at $M_{\rm BH} \approx 10^{(8\pm1)}$ M$_\odot$, and erroneously recover a single log-linear relation.

When Graham (2012) pointed out this overlooked inconsistency, he identified two different populations of galaxies, namely the core-Sérsic (Graham et al. 2003; Trujillo et al. 2004) and Sérsic spheroids[1], and attributed the

gsavorgn@astro.swin.edu.au

[1] Core-Sérsic spheroids have partially depleted cores relative to their outer Sérsic light profile, whereas Sérsic spheroids have no

change in slope (from log-quadratic to log-linear) to their different formation mechanisms. In this scenario, core-Sérsic spheroids are built in additive dry merger events, where the black hole and the bulge grow at the same pace, increasing their mass in lock steps ($M_{\rm BH} \propto L^{1}_{\rm sph}$), whereas Sérsic spheroids originate from gas-rich processes, in which the mass of the black hole increases more rapidly than the mass of its host spheroid ($M_{\rm BH} \propto L^{2.5}_{\rm sph}$). Graham & Scott (2013) and Scott et al. (2013) presented double power-law linear regressions for Sérsic/core-Sérsic spheroids in the $M_{\rm BH}-L_{\rm sph}$ and $M_{\rm BH}-M_{*,\rm sph}$ (spheroid stellar mass) diagrams, respectively, probing down to $M_{\rm BH} \approx 10^6$ M$_\odot$. To obtain their dust-corrected *bulge* magnitudes, they did not perform bulge/disc decompositions, but instead they converted $B-$band and K_S-band observed, total *galaxy* magnitudes using a mean statistical correction based on each object's morphological type and disc inclination[2]. It should be noted that ∼80% of their core-Sérsic spheroids were morphologically classified as elliptical galaxies, and ∼80% of their Sérsic spheroids were morphologically classified as bulges of disk galaxies (lenticulars and spirals).

Several recent papers (Jiang et al. 2011, 2013; Mathur et al. 2012; Reines et al. 2013) claimed an offset at the low-mass end of the $M_{\rm BH} - M_{*,\rm sph}$ diagram, such that the black hole mass is lower than expected from the near-linear correlation traced by the high-mass, early-type spheroids. However, Graham & Scott (2015) showed that the low-mass spheroids ($10^{8.5} \lesssim M_{*,\rm sph}/{\rm M}_\odot \lesssim 10^{10.5}$) are not randomly offset from the high-mass, near-linear correlation, but lie on the two times steeper relation traced by the Sérsic spheroids.

Here we investigate substructure in the $M_{\rm BH} - L_{\rm sph}$ and $M_{\rm BH} - M_{*,\rm sph}$ diagrams using state-of-the-art galaxy decompositions (Savorgnan & Graham *in preparation*, hereafter *Paper I*) for the largest sample of galaxies with directly measured black hole masses. Our decompositions were obtained from 3.6 μm *Spitzer* satellite imagery, which is an excellent proxy for the stellar mass, superior to the $K-$band (Sheth et al. 2010 and references therein). Nine of our galaxies have $M_{\rm BH} \lesssim 10^7$ M$_\odot$, which allows us to accurately constrain the slope of the correlation at the low-mass end. In addition to this, our galaxy sample includes 17 spiral galaxies, representing a notable improvement over the past studies dominated by early-type systems.

2. DATA

Our galaxy sample (see Table 1) consists of 66 objects for which a dynamical measurement of the black hole mass had been reported in the literature (Graham & Scott 2013; Rusli et al. 2013b) at the time we started this project, and for which we were able to obtain useful bulge parameters from 3.6 μm *Spitzer* satellite imagery. Bulge magnitudes were derived from our state-of-the-art galaxy decompositions, which take into account bulges, disks, spiral arms, bars, rings, haloes, extended or unresolved nuclear sources and partially depleted cores. Kinematical information (Emsellem et al. 2011; Scott et al. 2014; Arnold et al. 2014) was used to confirm the presence of rotationally supported components in most early-type galaxies, and to identify their extent (intermediate-scale, embedded disks or large-scale disks). *Paper I* will present the dataset used here to investigate the $M_{\rm BH} - L_{\rm sph}$ and $M_{\rm BH} - M_{*,\rm sph}$ diagrams, give details about the data reduction process and the sophisticated galaxy modelling technique that we developed, discuss how we estimated the uncertainties on the bulge parameters, and illustrate the individual 66 galaxy decompositions.

Bulge luminosities[3] were converted into stellar masses using the colour-$\Gamma_{3.6}$ relation published by Meidt et al. (2014, their equation 4), which allows one to estimate the 3.6 μm mass-to-light ratio, $\Gamma_{3.6}$, of a galaxy from its $[3.6]-[4.5]$ colour. Individual $[3.6]-[4.5]$ colours[4] were taken from Peletier et al. (2012, column 8 of their Table 1) when available for our galaxies, or were estimated from the bulge stellar velocity dispersion, σ, using the colour-σ relation presented by Peletier et al. (2012, their Figure 6). We point out here that using a single $\Gamma_{3.6} = 0.6$, independent of $[3.6]-[4.5]$ colour, does not significantly affect the results of our analysis.

The Sérsic/core-Sérsic classification presented in this work comes from the compilation of Savorgnan & Graham (2014), who identified partially depleted cores according to the same criteria used by Graham & Scott (2013). When no high-resolution image analysis was available from the literature, they inferred the presence of a partially depleted core based on the stellar velocity dispersion: a galaxy is classified as core-Sérsic if $\sigma > 270$ km s^{-1}, or as Sérsic if $\sigma < 166$ km s^{-1}.

For each galaxy, the total luminosity (or galaxy luminosity) is the sum of the luminosities of all its subcomponents. Due to the complexity of their modelling, four galaxies (see Table 1, column 7) had their galaxy luminosities underestimated[5], which are given here as lower limits.

3. ANALYSIS

4. RESULTS

compare scatter mbh-msph and mbh-mgal for early types

if 2 overmassive bhs removed, what happens?

5. CONCLUSIONS

This research was supported by Australian Research Council funding through grants DP110103509 and FT110100263. This work is based on observations made with the IRAC instrument (Fazio et al. 2004) on-board the Spitzer Space Telescope, which is operated by the Jet

central deficit of stars. While core-Sérsic spheroids are also "core galaxies", as given by the Nuker definition (Lauer et al. 2007b), it should be noted that ∼20% of "core galaxies" are not core-Sérsic spheroids (Dullo & Graham 2014, their Appendix A.2), i.e. do not have depleted cores. The change in slope of the $L_{\rm sph} - \sigma$ relation corresponds to the division between core-Sérsic and Sérsic spheroids (e.g. Graham & Guzmán 2003).

[2] While this resulted in individual bulge magnitudes not being exactly correct, their large sample size allowed them to obtain a reasonably ensemble average correction.

[3] Absolute luminosities were calculated assuming a 3.6 μm solar absolute magnitude of 3.25 mag (Sani et al. 2011).

[4] These are integrated $[3.6]-[4.5]$ colours, measured in a circular aperture within one galaxy's effective radius.

[5] These four cases will be discussed in *Paper I*.

TABLE 1

Galaxy sample. *Column (1):* Galaxy name. *Column (2):* Morphological type. *Column (3):* Presence of a partially depleted core. The question mark is used when the classification has come from the velocity dispersion criteria mentioned in Section 2. *Column (4):* Distance. *Column (5):* Black hole mass. *Column (6):* Absolute 3.6 μm bulge magnitude. *Column (7):* Absolute 3.6 μm galaxy magnitude. The four galaxy magnitudes marked with a * are lower limits. *Column (8):* [3.6] − [4.5] colour. *Column (9):* Bulge stellar mass.

Galaxy	**Type**	**Core**	**Distance**	$M_{\mathbf{BH}}$	$MAG_{\mathbf{sph}}$	$MAG_{\mathbf{gal}}$	**[3.6] − [4.5]**	$M_{\mathbf{*,sph}}$
			[Mpc]	[10^8 M$_\odot$]	[mag]	[mag]	[mag]	[10^{10} M$_\odot$]
(1)	(2)	(3)	(4)	(5)	(6)	(7)	(8)	(9)
IC 1459	E	yes	28.4	24^{+10}_{-10}	$-26.15^{+0.18}_{-0.11}$	−26.15	−0.12	27^{+30}_{-23}
IC 2560	S	no?	40.7	$0.044^{+0.044}_{-0.022}$	$-22.27^{+0.66}_{-0.58}$	−24.76	−0.08	$1.0^{+1.8}_{-0.6}$
IC 4296	E	yes?	40.7	11^{+2}_{-2}	$-26.35^{+0.18}_{-0.11}$	−26.35	−0.12	31^{+34}_{-26}
M104	S0/S	yes	9.5	$6.4^{+0.4}_{-0.4}$	$-23.91^{+0.66}_{-0.58}$	−25.21	−0.12	$3.4^{+5.8}_{-1.9}$
M105	E	yes	10.3	4^{+1}_{-1}	$-24.29^{+0.66}_{-0.58}$	−24.29	−0.10	$5.6^{+9.5}_{-3.0}$
M106	S	no	7.2	$0.39^{+0.01}_{-0.01}$	$-21.11^{+0.18}_{-0.11}$	−24.04	−0.08	$0.37^{+0.41}_{-0.31}$
M31	S	no	0.7	$1.4^{+0.9}_{-0.3}$	$-22.74^{+0.18}_{-0.11}$	−24.67	−0.09	$1.5^{+1.6}_{-1.3}$
M49	E	yes	17.1	25^{+3}_{-1}	$-26.54^{+0.18}_{-0.11}$	−26.54	−0.12	39^{+43}_{-33}
M59	E	no	17.8	$3.9^{+0.4}_{-0.4}$	$-25.18^{+0.18}_{-0.11}$	−25.27	−0.09	14^{+15}_{-11}
M64	S	no?	7.3	$0.016^{+0.004}_{-0.004}$	$-21.54^{+0.18}_{-0.11}$	−24.24	−0.06	$0.64^{+0.71}_{-0.55}$
M81	S	no	3.8	$0.74^{+0.21}_{-0.11}$	$-23.01^{+0.88}_{-0.66}$	−24.43	−0.09	$1.9^{+3.6}_{-0.9}$
M84	E	yes	17.9	$9.0^{+0.9}_{-0.8}$	$-26.01^{+0.66}_{-0.58}$	−26.01	−0.10	28^{+47}_{-15}
M87	E	yes	15.6	$58.0^{+3.5}_{-3.5}$	$-26.00^{+0.66}_{-0.58}$	−26.00	−0.11	26^{+44}_{-14}
M89	E	yes	14.9	$4.7^{+0.5}_{-0.5}$	$-24.48^{+0.66}_{-0.58}$	−24.74	−0.11	$6.3^{+10.7}_{-3.4}$
M94	S	no?	4.4	$0.060^{+0.014}_{-0.014}$	$-22.08^{+0.18}_{-0.11}$	−23.36 *	−0.07	$1.00^{+1.11}_{-0.85}$
M96	S	no	10.1	$0.073^{+0.015}_{-0.015}$	$-22.15^{+0.18}_{-0.11}$	−24.20	−0.08	$0.97^{+1.08}_{-0.83}$
NGC 0524	S0	yes	23.3	$8.3^{+2.7}_{-1.3}$	$-23.19^{+0.18}_{-0.11}$	−24.92	−0.09	$2.2^{+2.5}_{-1.9}$
NGC 0821	E	no	23.4	$0.39^{+0.26}_{-0.09}$	$-24.00^{+0.88}_{-0.66}$	−24.26	−0.09	$4.7^{+8.7}_{-2.1}$
NGC 1023	S0	no	11.1	$0.42^{+0.04}_{-0.04}$	$-22.82^{+0.18}_{-0.11}$	−24.20	−0.10	$1.5^{+1.7}_{-1.3}$
NGC 1300	S	no	20.7	$0.73^{+0.69}_{-0.35}$	$-22.06^{+0.66}_{-0.58}$	−24.16	−0.10	$0.70^{+1.19}_{-0.38}$
NGC 1316	merger	no	18.6	$1.50^{+0.75}_{-0.80}$	$-24.89^{+0.66}_{-0.58}$	−26.48	−0.10	$9.5^{+16.2}_{-5.2}$
NGC 1332	E/S0	no	22.3	14^{+2}_{-2}	$-24.89^{+0.88}_{-0.66}$	−24.95	−0.12	$8.2^{+15.0}_{-3.6}$
NGC 1374	E	no?	19.2	$5.8^{+0.5}_{-0.5}$	$-23.68^{+0.18}_{-0.11}$	−23.70	−0.09	$3.6^{+4.0}_{-3.0}$
NGC 1399	E	yes	19.4	$4.7^{+0.6}_{-0.6}$	$-26.43^{+0.18}_{-0.11}$	−26.46	−0.12	33^{+37}_{-28}
NGC 2273	S	no	28.5	$0.083^{+0.004}_{-0.004}$	$-23.00^{+0.66}_{-0.58}$	−24.21	−0.08	$2.0^{+3.4}_{-1.1}$
NGC 2549	S0	no	12.3	$0.14^{+0.02}_{-0.13}$	$-21.25^{+0.18}_{-0.11}$	−22.60	−0.10	$0.35^{+0.39}_{-0.30}$
NGC 2778	S0	no	22.3	$0.15^{+0.09}_{-0.10}$	$-20.80^{+0.66}_{-0.58}$	−22.44	−0.09	$0.25^{+0.43}_{-0.14}$
NGC 2787	S0	no	7.3	$0.40^{+0.04}_{-0.05}$	$-20.11^{+0.66}_{-0.58}$	−22.28	−0.10	$0.12^{+0.20}_{-0.07}$
NGC 2974	S	no	20.9	$1.7^{+0.2}_{-0.2}$	$-22.95^{+0.66}_{-0.58}$	−24.16	−0.09	$1.8^{+3.1}_{-1.0}$
NGC 3079	S	no?	20.7	$0.024^{+0.024}_{-0.012}$	$-23.01^{+0.66}_{-0.58}$	−24.45 *	−0.07	$2.4^{+4.0}_{-1.3}$
NGC 3091	E	yes	51.2	36^{+1}_{-2}	$-26.28^{+0.18}_{-0.11}$	−26.28	−0.12	30^{+34}_{-26}
NGC 3115	E/S0	no	9.4	$8.8^{+10.0}_{-2.7}$	$-24.22^{+0.18}_{-0.11}$	−24.40	−0.11	$4.9^{+5.4}_{-4.1}$
NGC 3227	S	no	20.3	$0.14^{+0.10}_{-0.06}$	$-21.76^{+0.66}_{-0.58}$	−24.26	−0.08	$0.67^{+1.15}_{-0.37}$
NGC 3245	S0	no	20.3	$2.0^{+0.5}_{-0.5}$	$-22.43^{+0.18}_{-0.11}$	−23.88	−0.10	$1.0^{+1.1}_{-0.9}$
NGC 3377	E	no	10.9	$0.77^{+0.04}_{-0.06}$	$-23.49^{+0.66}_{-0.58}$	−23.57	−0.06	$4.0^{+6.8}_{-2.2}$
NGC 3384	S0	no	11.3	$0.17^{+0.01}_{-0.02}$	$-22.43^{+0.18}_{-0.11}$	−23.74	−0.08	$1.2^{+1.3}_{-1.0}$
NGC 3393	S	no	55.2	$0.34^{+0.02}_{-0.02}$	$-23.48^{+0.66}_{-0.58}$	−25.29	−0.10	$2.8^{+4.7}_{-1.5}$
NGC 3414	E	no	24.5	$2.4^{+0.3}_{-0.3}$	$-24.35^{+0.18}_{-0.11}$	−24.42	−0.09	$6.5^{+7.2}_{-5.5}$
NGC 3489	S0/S	no	11.7	$0.058^{+0.008}_{-0.008}$	$-21.13^{+0.66}_{-0.58}$	−23.07	−0.06	$0.42^{+0.72}_{-0.23}$
NGC 3585	E	no	19.5	$3.1^{+1.4}_{-0.6}$	$-25.52^{+0.66}_{-0.58}$	−25.55	−0.10	18^{+30}_{-10}
NGC 3607	E	no	22.2	$1.3^{+0.5}_{-0.5}$	$-25.36^{+0.66}_{-0.58}$	−25.45	−0.10	15^{+25}_{-8}
NGC 3608	E	yes	22.3	$2.0^{+1.1}_{-0.6}$	$-24.50^{+0.66}_{-0.58}$	−24.50	−0.08	$7.8^{+13.4}_{-4.3}$
NGC 3842	E	yes	98.4	97^{+30}_{-26}	$-27.00^{+0.18}_{-0.11}$	−27.04	−0.11	61^{+68}_{-52}
NGC 3998	S0	no	13.7	$8.1^{+2.0}_{-1.9}$	$-22.32^{+0.88}_{-0.66}$	−23.53	−0.12	$0.78^{+1.43}_{-0.35}$
NGC 4026	S0	no	13.2	$1.8^{+0.6}_{-0.3}$	$-21.58^{+0.88}_{-0.66}$	−23.16	−0.09	$0.50^{+0.92}_{-0.22}$
NGC 4151	S	no	20.0	$0.65^{+0.07}_{-0.07}$	$-23.40^{+0.66}_{-0.58}$	−24.44	−0.09	$2.8^{+4.8}_{-1.5}$
NGC 4261	E	yes	30.8	5^{+1}_{-1}	$-25.72^{+0.66}_{-0.58}$	−25.76	−0.12	18^{+30}_{-10}
NGC 4291	E	yes	25.5	$3.3^{+0.9}_{-2.5}$	$-24.05^{+0.66}_{-0.58}$	−24.05	−0.11	$3.9^{+6.7}_{-2.1}$
NGC 4388	S	no?	17.0	$0.075^{+0.002}_{-0.002}$	$-21.26^{+0.88}_{-0.66}$	−23.50 *	−0.07	$0.46^{+0.85}_{-0.21}$
NGC 4459	S0	no	15.7	$0.68^{+0.13}_{-0.13}$	$-23.48^{+0.66}_{-0.58}$	−24.01	−0.09	$2.9^{+5.0}_{-1.6}$

Galaxy	**Type**	**Core**	**Distance**	$M_{\rm BH}$	$MAG_{\rm sph}$	$MAG_{\rm gal}$	$[3.6]-[4.5]$	$M_{*,\rm sph}$
			[Mpc]	[10^8 M$_\odot$]	[mag]	[mag]	[mag]	[10^{10} M$_\odot$]
(1)	(2)	(3)	(4)	(5)	(6)	(7)	(8)	(9)
NGC 4473	E	no	15.3	$1.2^{+0.4}_{-0.9}$	$-23.88^{+0.66}_{-0.58}$	-24.11	-0.10	$3.9^{+6.6}_{-2.1}$
NGC 4564	S0	no	14.6	$0.60^{+0.03}_{-0.09}$	$-22.30^{+0.18}_{-0.11}$	-22.99	-0.11	$0.82^{+0.91}_{-0.70}$
NGC 4596	S0	no	17.0	$0.79^{+0.38}_{-0.33}$	$-22.73^{+0.18}_{-0.11}$	-24.18	-0.08	$1.6^{+1.7}_{-1.3}$
NGC 4697	E	no	11.4	$1.8^{+0.2}_{-0.1}$	$-24.82^{+0.88}_{-0.66}$	-24.94	-0.09	10^{+18}_{-4}
NGC 4889	E	yes	103.2	210^{+160}_{-160}	$-27.54^{+0.18}_{-0.11}$	-27.54	-0.12	91^{+101}_{-77}
NGC 4945	S	no?	3.8	$0.014^{+0.014}_{-0.007}$	$-20.96^{+0.66}_{-0.58}$	-23.79 *	-0.06	$0.36^{+0.62}_{-0.20}$
NGC 5077	E	yes	41.2	$7.4^{+4.7}_{-3.0}$	$-25.45^{+0.18}_{-0.11}$	-25.45	-0.11	15^{+17}_{-13}
NGC 5128	merger	no?	3.8	$0.45^{+0.17}_{-0.10}$	$-23.89^{+0.88}_{-0.66}$	-24.97	-0.07	$5.0^{+9.1}_{-2.2}$
NGC 5576	E	no	24.8	$1.6^{+0.3}_{-0.4}$	$-24.44^{+0.18}_{-0.11}$	-24.44	-0.09	$7.1^{+7.9}_{-6.0}$
NGC 5845	S0	no	25.2	$2.6^{+0.4}_{-1.5}$	$-22.96^{+0.88}_{-0.66}$	-23.10	-0.12	$1.4^{+2.6}_{-0.6}$
NGC 5846	E	yes	24.2	11^{+1}_{-1}	$-25.81^{+0.66}_{-0.58}$	-25.81	-0.10	22^{+38}_{-12}
NGC 6251	E	yes?	104.6	5^{+2}_{-2}	$-26.75^{+0.18}_{-0.11}$	-26.75	-0.12	46^{+51}_{-39}
NGC 7052	E	yes	66.4	$3.7^{+2.6}_{-1.5}$	$-26.32^{+0.18}_{-0.11}$	-26.32	-0.11	33^{+36}_{-28}
NGC 7619	E	yes	51.5	25^{+8}_{-3}	$-26.35^{+0.66}_{-0.58}$	-26.41	-0.11	33^{+56}_{-18}
NGC 7768	E	yes	112.8	13^{+5}_{-4}	$-26.90^{+0.66}_{-0.58}$	-26.90	-0.11	57^{+98}_{-31}
UGC 03789	S	no?	48.4	$0.108^{+0.005}_{-0.005}$	$-22.77^{+0.88}_{-0.66}$	-24.20	-0.07	$1.9^{+3.4}_{-0.8}$

TABLE 2
Linear regression analysis.

Subsample (size)	Regression	α	β	X_0	ϵ	Δ
		$\log[M_{\rm BH}/{\rm M}_\odot] = \alpha + \beta[(MAG_{\rm sph} - X_0)/{\rm mag}]$				
All (66)	BCES OLS($Y\|X$)	8.16 ± 0.07	-0.44 ± 0.04	-23.86	–	0.56
	BCES OLS($X\|Y$)	8.16 ± 0.08	-0.61 ± 0.05	-23.86	–	0.68
	BCES Bisector	8.16 ± 0.07	-0.52 ± 0.04	-23.86	–	0.60
	FITEXY OLS($Y\|X$)	$8.17^{+0.07}_{-0.06}$	$-0.43^{+0.03}_{-0.03}$	-23.86	0.49	0.56
	FITEXY OLS($X\|Y$)	$8.15^{+0.07}_{-0.07}$	$-0.61^{+0.04}_{-0.05}$	-23.86	0.96	0.67
	FITEXY Bisector	$8.16^{+0.07}_{-0.07}$	$-0.51^{+0.04}_{-0.04}$	-23.86	–	0.60
Core-Sérsic (22)	BCES OLS($Y\|X$)	9.06 ± 0.09	-0.3 ± 0.1	-25.73	–	0.42
	BCES OLS($X\|Y$)	9.1 ± 0.1	-0.6 ± 0.1	-25.73	–	0.61
	BCES Bisector	9.1 ± 0.1	-0.47 ± 0.08	-25.73	–	0.48
	FITEXY OLS($Y\|X$)	$9.06^{+0.09}_{-0.08}$	$-0.26^{+0.07}_{-0.08}$	-25.73	0.37	0.42
	FITEXY OLS($X\|Y$)	$9.0^{+0.1}_{-0.1}$	$-0.7^{+0.2}_{-0.3}$	-25.73	0.85	0.67
	FITEXY Bisector	$9.0^{+0.1}_{-0.1}$	$-0.5^{+0.1}_{-0.2}$	-25.73	–	0.48
Sérsic (44)	BCES OLS($Y\|X$)	7.71 ± 0.09	-0.41 ± 0.08	-22.92	–	0.61
	BCES OLS($X\|Y$)	7.7 ± 0.1	-0.9 ± 0.2	-22.92	–	0.93
	BCES Bisector	7.7 ± 0.1	-0.61 ± 0.08	-22.92	–	0.71
	FITEXY OLS($Y\|X$)	$7.72^{+0.08}_{-0.08}$	$-0.41^{+0.07}_{-0.07}$	-22.92	0.54	0.61
	FITEXY OLS($X\|Y$)	$7.7^{+0.1}_{-0.1}$	$-0.9^{+0.1}_{-0.2}$	-22.92	0.89	0.93
	FITEXY Bisector	$7.7^{+0.1}_{-0.1}$	$-0.61^{+0.09}_{-0.12}$	-22.92	–	0.71
Early-type (E+S0) (45)	BCES OLS($Y\|X$)	8.56 ± 0.07	-0.33 ± 0.04	-24.47	–	0.46
	BCES OLS($X\|Y$)	8.56 ± 0.08	-0.48 ± 0.05	-24.47	–	0.55
	BCES Bisector	8.56 ± 0.07	-0.40 ± 0.04	-24.47	–	0.49
	FITEXY OLS($Y\|X$)	$8.56^{+0.06}_{-0.06}$	$-0.32^{+0.03}_{-0.04}$	-24.47	0.40	0.46
	FITEXY OLS($X\|Y$)	$8.54^{+0.08}_{-0.08}$	$-0.49^{+0.05}_{-0.06}$	-24.47	1.00	0.57
	FITEXY Bisector	$8.55^{+0.07}_{-0.07}$	$-0.41^{+0.04}_{-0.05}$	-24.47	–	0.49
Late-type (S) (17)	BCES OLS($Y\|X$)	7.2 ± 0.2	-0.8 ± 0.4	-22.33	–	0.70
	BCES OLS($X\|Y$)	7.2 ± 0.3	-1.7 ± 0.7	-22.33	–	1.26
	BCES Bisector	7.2 ± 0.2	-1.1 ± 0.3	-22.33	–	0.88
	FITEXY OLS($Y\|X$)	$7.2^{+0.1}_{-0.1}$	$-0.5^{+0.2}_{-0.2}$	-22.33	0.54	0.63
	FITEXY OLS($X\|Y$)	$7.4^{+0.5}_{-0.3}$	$-2.0^{+0.7}_{-2.3}$	-22.33	0.54	1.51
	FITEXY Bisector	$7.3^{+0.4}_{-0.3}$	$-1.0^{+0.3}_{-0.5}$	-22.33	–	0.82
		$\log[M_{\rm BH}/{\rm M}_\odot] = \alpha + \beta[(MAG_{\rm gal} - X_0)/{\rm mag}]$				
All (62)	BCES OLS($Y\|X$)	8.26 ± 0.08	-0.49 ± 0.06	-24.78	–	0.64
	BCES OLS($X\|Y$)	8.3 ± 0.1	-1.0 ± 0.1	-24.78	–	0.92
	BCES Bisector	8.26 ± 0.09	-0.72 ± 0.07	-24.78	–	0.71
	FITEXY OLS($Y\|X$)	$8.26^{+0.08}_{-0.08}$	$-0.48^{+0.06}_{-0.07}$	-24.78	0.62	0.64
	FITEXY OLS($X\|Y$)	$8.3^{+0.1}_{-0.1}$	$-1.0^{+0.1}_{-0.2}$	-24.78	0.87	0.93
	FITEXY Bisector	$8.3^{+0.1}_{-0.1}$	$-0.72^{+0.08}_{-0.10}$	-24.78	–	0.71
Early-type (E+S0) (45)	BCES OLS($Y\|X$)	8.56 ± 0.06	-0.43 ± 0.05	-24.88	–	0.45
	BCES OLS($X\|Y$)	8.56 ± 0.08	-0.63 ± 0.05	-24.88	–	0.53
	BCES Bisector	8.56 ± 0.07	-0.53 ± 0.04	-24.88	–	0.47
	FITEXY OLS($Y\|X$)	$8.56^{+0.06}_{-0.06}$	$-0.41^{+0.05}_{-0.05}$	-24.88	0.41	0.45
	FITEXY OLS($X\|Y$)	$8.56^{+0.07}_{-0.09}$	$-0.66^{+0.06}_{-0.08}$	-24.88	0.79	0.55
	FITEXY Bisector	$8.56^{+0.07}_{-0.07}$	$-0.53^{+0.05}_{-0.07}$	-24.88	–	0.47

Propulsion Laboratory, California Institute of Technology under a contract with NASA. This research has made use of the GOLDMine database (Gavazzi et al. 2003) and the NASA/IPAC Extragalactic Database (NED) which is operated by the Jet Propulsion Laboratory, California Institute of Technology, under contract with the National Aeronautics and Space Administration.

REFERENCES

Arnold, J. A., Romanowsky, A. J., Brodie, J. P., et al. 2014, ApJ, 791, 80
Balcells, M., Graham, A. W., & Peletier, R. F. 2007, ApJ, 665, 1104
Beifiori, A., Courteau, S., Corsini, E. M., & Zhu, Y. 2012, MNRAS, 419, 2497
Chilingarian, I. V., Cayatte, V., Durret, F., et al. 2008, A&A, 486, 85
Cody, A. M., Carter, D., Bridges, T. J., Mobasher, B., & Poggianti, B. M. 2009, MNRAS, 396, 1647
Davies, R. L., Efstathiou, G., Fall, S. M., Illingworth, G., & Schechter, P. L. 1983, ApJ, 266, 41
de Rijcke, S., Michielsen, D., Dejonghe, H., Zeilinger, W. W., & Hau, G. K. T. 2005, A&A, 438, 491
Dressler, A. 1989, in IAU Symposium, Vol. 134, Active Galactic Nuclei, ed. D. E. Osterbrock & J. S. Miller, 217
Dullo, B. T., & Graham, A. W. 2014, MNRAS, 444, 2700
Emsellem, , & E. et al. 2011, MNRAS, 414, 888
Erwin, P., & Gadotti, D. A. 2012, Advances in Astronomy, 2012, 4
Fazio, G. G., Hora, J. L., Allen, L. E., et al. 2004, ApJS, 154, 10
Ferrarese, L., & Ford, H. 2005, Space Sci. Rev., 116, 523
Ferrarese, L., & Merritt, D. 2000, ApJ, 539, L9
Forbes, D. A., Lasky, P., Graham, A. W., & Spitler, L. 2008, MNRAS, 389, 1924

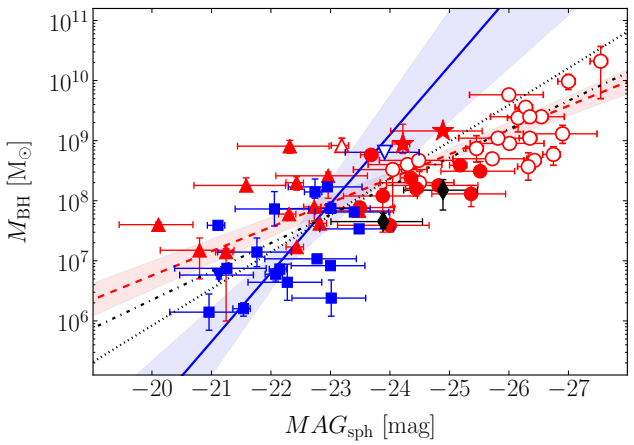

FIG. 1.— Black hole mass against 3.6 μm spheroid absolute magnitude. Symbols are coded according to the galaxy morphological type: red circle = elliptical, red star = elliptical/lenticular, red upward triangle = lenticular, blue downward triangle = lenticular/spiral, blue square = spiral, black diamond = merger. Empty symbols represent core-Sérsic spheroids, whereas filled symbols are used for Sérsic spheroids. The red dashed line indicates the BCES bisector linear regression for early-type galaxies (ellipticals+lenticulars), with the red shaded area denoting its 1σ uncertainty. The blue solid line shows the BCES bisector linear regression for spiral galaxies, with the blue shaded area denoting its 1σ uncertainty. The black dashed-dotted and dotted lines represent the BCES bisector linear regressions for core-Sérsic and Sérsic spheroids, respectively.

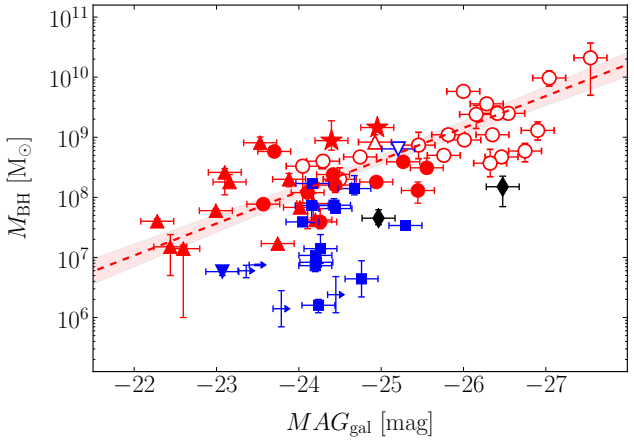

FIG. 2.— Black hole mass against 3.6 μm galaxy absolute magnitude. Symbols are coded as in Figure 1. Four spiral galaxies had their magnitudes overestimated and are shown as upper limits.

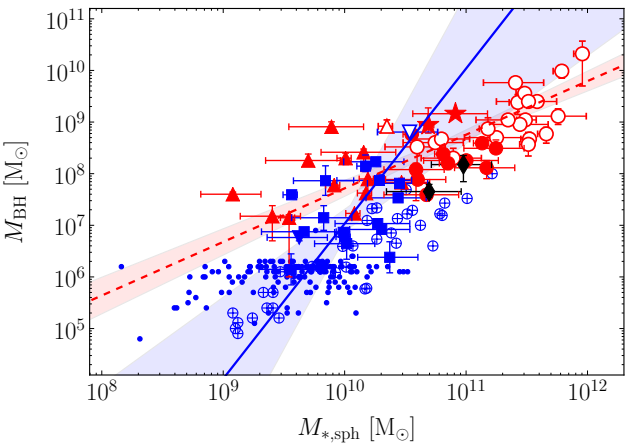

FIG. 3.— Black hole mass against spheroid stellar mass. Symbols are coded as in Figure 1, with the addition of the blue dots representing **the AGN sample Jiang**, and the blue crossed circles denoting **the other AGNs**. The red dashed line indicates the BCES bisector linear regression for early-type galaxies (ellipticals+lenticulars), with the red shaded area denoting its 1σ uncertainty. The blue solid line shows the BCES bisector linear regression for spiral galaxies, with the blue shaded area denoting its 1σ uncertainty.

Gavazzi, G., Boselli, A., Donati, A., Franzetti, P., & Scodeggio, M. 2003, A&A, 400, 451
Gebhardt, K., Bender, R., Bower, G., et al. 2000, ApJ, 539, L13
Graham, A. W. 2007, MNRAS, 379, 711
—. 2008, PASA, 25, 167
—. 2012, ApJ, 746, 113
—. 2015, ArXiv e-prints, arXiv:1501.02937
Graham, A. W., Erwin, P., Trujillo, I., & Asensio Ramos, A. 2003, AJ, 125, 2951
Graham, A. W., & Guzmán, R. 2003, AJ, 125, 2936
Graham, A. W., Onken, C. A., Athanassoula, E., & Combes, F. 2011, MNRAS, 412, 2211
Graham, A. W., & Scott, N. 2013, ApJ, 764, 151
—. 2015, ApJ, 798, 54
Gültekin, K., Richstone, D. O., Gebhardt, K., et al. 2009, ApJ, 698, 198
Häring, N., & Rix, H.-W. 2004, ApJ, 604, L89
Held, E. V., de Zeeuw, T., Mould, J., & Picard, A. 1992, in IAU Symposium, Vol. 149, The Stellar Populations of Galaxies, ed. B. Barbuy & A. Renzini, 429
Jiang, N., Ho, L. C., Dong, X.-B., Yang, H., & Wang, J. 2013, ApJ, 770, 3
Jiang, Y.-F., Greene, J. E., & Ho, L. C. 2011, ApJ, 737, L45
Kormendy, J., & Ho, L. C. 2013, ARA&A, 51, 511
Kormendy, J., & Richstone, D. 1995, ARA&A, 33, 581
Kourkchi, E., Khosroshahi, H. G., Carter, D., et al. 2012, MNRAS, 420, 2819
Laor, A. 1998, ApJ, 505, L83
—. 2001, ApJ, 553, 677
Läsker, R., Ferrarese, L., & van de Ven, G. 2014a, ApJ, 780, 69
Läsker, R., Ferrarese, L., van de Ven, G., & Shankar, F. 2014b, ApJ, 780, 70
Lauer, T. R., Faber, S. M., Richstone, D., et al. 2007a, ApJ, 662, 808
—. 2007b, ApJ, 662, 808
Liu, F. S., Xia, X. Y., Mao, S., Wu, H., & Deng, Z. G. 2008, MNRAS, 385, 23
Magorrian, J., Tremaine, S., Richstone, D., et al. 1998, AJ, 115, 2285
Malumuth, E. M., & Kirshner, R. P. 1981, ApJ, 251, 508
Marconi, A., & Hunt, L. K. 2003, ApJ, 589, L21
Mathur, S., Fields, D., Peterson, B. M., & Grupe, D. 2012, ApJ, 754, 146
Matković, A., & Guzmán, R. 2005, MNRAS, 362, 289
McConnell, N. J., & Ma, C.-P. 2013, ApJ, 764, 184
McConnell, N. J., Ma, C.-P., Gebhardt, K., et al. 2011, Nature, 480, 215
Meidt, S. E., Schinnerer, E., van de Ven, G., et al. 2014, ApJ, 788, 144
Peletier, R. F., Kutdemir, E., van der Wolk, G., et al. 2012, MNRAS, 419, 2031
Reines, A. E., Greene, J. E., & Geha, M. 2013, ApJ, 775, 116
Rusli, S. P., Erwin, P., Saglia, R. P., et al. 2013a, AJ, 146, 160
Rusli, S. P., Thomas, J., Saglia, R. P., et al. 2013b, AJ, 146, 45
Ryan, C. J., De Robertis, M. M., Virani, S., Laor, A., & Dawson, P. C. 2007, ApJ, 654, 799
Sani, E., Marconi, A., Hunt, L. K., & Risaliti, G. 2011, MNRAS, 413, 1479

Savorgnan, G. A. D., & Graham, A. W. 2014, ArXiv e-prints, arXiv:1410.7405
Schechter, P. L. 1980, AJ, 85, 801
Scott, N., Davies, R. L., Houghton, R. C. W., et al. 2014, MNRAS, 441, 274
Scott, N., Graham, A. W., & Schombert, J. 2013, ApJ, 768, 76
Sheth, K., Regan, M., Hinz, J. L., et al. 2010, PASP, 122, 1397
Tortora, C., Napolitano, N. R., Romanowsky, A. J., Capaccioli, M., & Covone, G. 2009, MNRAS, 396, 1132
Trujillo, I., Erwin, P., Asensio Ramos, A., & Graham, A. W. 2004, AJ, 127, 1917
van den Bosch, R. C. E., Gebhardt, K., Gültekin, K., et al. 2012, Nature, 491, 729
Vika, M., Driver, S. P., Cameron, E., Kelvin, L., & Robotham, A. 2012, MNRAS, 419, 2264
von der Linden, A., Best, P. N., Kauffmann, G., & White, S. D. M. 2007, MNRAS, 379, 867
Wandel, A. 1999, ApJ, 519, L39
Yee, H. K. C. 1992, in Astronomical Society of the Pacific Conference Series, Vol. 31, Relationships Between Active Galactic Nuclei and Starburst Galaxies, ed. A. V. Filippenko, 417